Fragmentation of Unstable Neutron-Rich Oxygen Beams

A. Leistenschneider[1], T. Aumann[2], K. Boretzky[3], L.F. Canto[7], B.V. Carlson[8], D. Cortina[2], U. Datta Pramanik[2],
Th.W. Elze[1], H. Emling[2], H. Geissel[2], A. Grünschloß[1], K. Helariutta[2], M. Hellström[2], M.S. Hussein[9], S. Ilievski[1,2],
K. Jones[2], J.V. Kratz[3], R. Kulessa[5], Le Hong Khiem[3], E. Lubkiewicz[5], G. Münzenberg[2], R. Palit[1], P. Reiter[6],
C. Scheidenberger[2], K.-H. Schmidt[2], H. Simon[4], K. Sümmerer[2], E. Wajda[5], W. Walús[5]

[1] *Institut für Kernphysik, Johann Wolfgang Goethe-Universität, D-60486 Frankfurt, Germany*
[2] *Gesellschaft für Schwerionenforschung (GSI), D-64291 Darmstadt, Germany*
[3] *Institut für Kernchemie, Johannes Gutenberg-Universität, D-55099 Mainz, Germany*
[4] *Institut für Kernphysik, Technische Universität, D-64289 Darmstadt, Germany*
[5] *Instytut Fizyki, Uniwersytet Jagelloński, PL-30-059 Kraków, Poland*
[6] *Sektion Physik, Ludwig-Maximilians-Universität, D-85748 Garching, Germany*
[7] *Instituto de Fisica, Universidade Federal do Rio de Janeiro, 21945-970 Rio de Janeiro, Brazil*
[8] *Departemento de Fisica, Instituto Tecnologico de Aeronautica - CTA, 12228-900 Sao Jose dos Campos, Brazil*
[9] *Instituto de Fisica, Universidade de Sao Paulo, 05389-970, Sao Paulo, Brazil*

Fragmentation of secondary beams of neutron-rich, unstable ^{19,20,21}O isotopes at beam energies near 600 MeV/nucleon was studied by measuring the production cross sections for carbon, nitrogen, and oxygen fragments. Data for stable ^{17,18}O beams were obtained as well. The measurements serve to illuminate the isospin dependence of the fragmentation process. The experimental results are compared to those from an empirical parameterization and to those from abrasion-ablation models.

PACS numbers: 25.60.+v,25.70.Mn,27.20.+n,27.30.+t

I. INTRODUCTION

Fragmentation of energetic heavy-ion beams is widely used to produce secondary beams of exotic nuclei far from stability [1]. In order to asses the feasibility of experiments utilizing secondary beams, a precise knowledge of the relevant production cross sections is mandatory. Usually, production cross sections are deduced from empirical parameterizations of measured cross sections, e.g., the frequently used EPAX parametrization [2]. Alternatively, fragmentation models with a microscopic background have been applied, such as 'abrasion-ablation' models [3–5] or 'intranuclear-cascade' simulations [6].

The validity of both, the empirical parameterization and the physical models, has been verified mainly for medium- to heavy-mass fragments (see, e.g., Refs. [2,7–10]. In particular, it could be shown that in the few cases where fragmentation cross sections of projectiles with different neutron-to-proton ratios were studied the observed shift of the centroids of the isotope distributions was rather well reproduced by EPAX (see Fig. 11 in Ref. [2]). The data are much too scarce, however, to investigate in detail how the shapes of the distributions, in addition to their centroids, vary with the neutron- or proton-excess of the projectiles.

Recently, two-step fragmentation processes were discussed in the context of an efficient production of very neutron-rich isotopes. This process involves an unstable neutron-rich fragment as an intermediate product which undergoes fragmentation again, yielding the final nucleus of interest Such two-step mechanisms were considered, in particular, in proposals for the next-generation exotic nuclear beam facilities [11–13]. On the basis of the EPAX parameterization, considerable gain factors for the pro-

duction of specific very neutron-rich isotopes in two-step fragmentation processes in comparison to one-step fragmentation were deduced. These findings, however, are in contrast to results obtained on the basis of an abrasion-ablation model [14].

Here, we report on a rather comprehensive fragmentation study of the unstable neutron-rich nuclei ^{19,20,21}O, together with that of the stable ^{17,18}O isotopes. The results can serve to illustrate the effect of isospin on the fragmentation process and thus help to clarify the above discrepancies between various predictions.

II. EXPERIMENTAL METHOD

Secondary beams of $^{17-21}$O ions were produced in a fragmentation reaction of a primary ^{40}Ar beam delivered by the synchrotron SIS at GSI, Darmstadt. The ^{40}Ar beam energy amounted to 720 MeV/nucleon and the intensity to about 10^{10} ions per second. A beryllium production target of 5 g/cm^2 thickness was used. The secondary oxygen beams were separated in the Fragment Separator FRS [15] operated at three different magnetic field settings optimized for ^{17,18}O, ^{19,20}O, and ^{21,22}O, respectively. Due to the low production cross section in the case of ^{22}O, the counting statistics was poor and no results will be reported. Though ^{17,18}O are stable isotopes, they were produced as secondary beams for economical reasons. Except for the setting optimized for ^{21,22}O, a shaped degrader in the FRS mid-plane was used in order to suppress abundant contaminants from elements other than oxygen. The kinetic energies of the secondary beams vary slightly around 600 MeV/nucleon and are quoted in Table I.

The secondary beams were transported to the experimental area where they were directed onto targets of ^{nat}C (0.573 g/cm^2) and ^{nat}Pb (1.820 g/cm^2); measurements without targets were also performed. The fragmentation measurement was performed in conjunction with experiments aiming at other subjects [16]; the detector setup will be discussed only as far as it is relevant for the present purpose.

The aim of this measurement was to determine cross sections for projectile fragmentation, the cross sections being differentiated with regard to the nuclear charge and mass of the produced fragments but integrated with regard to any other observable quantity. The applied method simply relies on counting the number of projectiles impinging on the target and counting the number of fragments produced. For that purpose, the incident projectiles needed to be identified uniquely on an event-by-event basis, likewise the fragments. Due to the high beam energy, the fragments are kinematically focussed into a rather narrow forward cone around the beam direction.

Identification and trajectories of the projectiles. Upstream from the target, the detector system consisted of three thin organic scintillation detectors, a silicon detector, and a 4-jaw slit built from 5 mm thick organic scintillation material. The slit, the silicon detector, and one of the scintillation detectors were placed close to the target, the other two scintillation detectors about 10 m and 90 m upstream from the target. The slit detector served to restrict the size of the beam spot on the target and thus to suppress the beam halo. Two of the scintillation detectors as well as the silicon detector were position sensitive. The scintillators were of quadratic shape covering an area of 50 x 50 mm^2. The scintillation light was collected from the four edges by means of light guides and detected by four phototubes. From the relative pulse height of the four signals the two-dimensional position information could be derived, the mean time signals of these detectors served to measure the velocities of the projectiles. The silicon detector with a resistive electrode also delivered two-dimensional position information and, in addition, a signal proportional to the energy loss of the projectile in the detector. From the latter signal, in combination with the velocity measurement, the nuclear charge Z_p of the projectile could be derived. From the known magnetic rigidity and the charge and velocity measurement, the mass of the projectile was obtained. Typical resolutions (one standard deviation) of 1 mm for position, 170 ps for time of flight, 0.2 e for nuclear charge, and 0.1 amu for the mass of the projectile were achieved.

Identification and trajectory of the fragments. Downstream from the target, the detection system for the fragments consisted of two silicon detectors (one of them being position sensitive), a dipole magnet with a large gap of 0.5 m x 1.2 m, three scintillating fiber detectors, and an array of 20 organic scintillation detectors (TFW), each
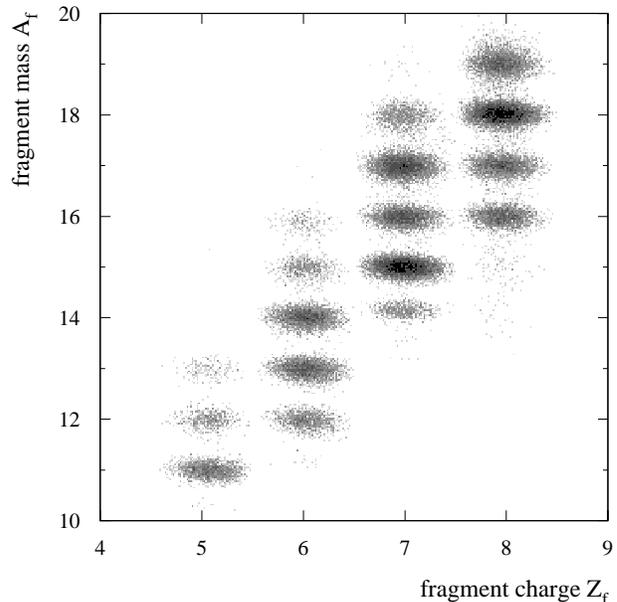

FIG. 1. Identification of fragments produced in reactions of a ^{20}O beam impinging on a carbon target.

one of 2000 x 100 x 10 mm^3 size and placed about 11 m downstream from the target. The trajectories of the fragments were traced by means of the position sensitive silicon detector and the scintillating fiber detectors. The velocities of the fragments were measured using TFW. Each of the TFW modules was equipped with two phototubes, the mean time signal of which determined the time of flight of each fragment. From the time-of-flight information the fragment velocity can be derived if corrections for energy losses along the flight path are applied. The nuclear charge of the fragment could be derived from the energy loss in the two silicon detectors, but also from that in TFW. The trajectories of the fragments measured in front of and behind the magnet determined their magnetic rigidities. This information in combination with the deduced charge and velocity allowed to determine the mass of the fragment. A mass resolution of 0.1 - 0.15 amu could be achieved. Fig. 1 shows the fragment mass (A_f) and charge (Z_f) distribution as obtained for the ^{20}O beam. In order to suppress non-interacting projectiles, the fragment distribution shown in this figure was accumulated requiring at least one neutron being emitted from the fragment and observed in a neutron detector in forward direction. This constraint, however, was not applied in the analysis of the fragment cross sections and is thus not discussed further.

The detector system was kept under vacuum up to the exit from the magnet about 3.5 m downstream from the target. Projectiles or fragments undergo nuclear interactions in the detector material or while travelling through air. To a large extent, such interactions could be discriminated by requiring that the nuclear charge measured in the two silicon detectors and in TFW is identical for all

three detectors within their resolutions. Residual background from interactions outside the target was determined by means of a measurement without target and was subtracted.

Each incident projectile delivered a trigger for the data aquisition. Depending on beam intensity, the trigger rate had to be scaled down in order to cope with the capability of the data aquisition system. The production cross section σ_f for a specific fragment was obtained from

$$\sigma_f = \frac{R_f c_f}{R_p c_p N_t}. \tag{1}$$

N_t denotes the number of target atoms per cm^2, R_p and R_f the rates of the identified projectiles and fragments, respectively. Certain corrections c_p and c_f had to be applied to R_p and R_f, respectively, in order to account for instrumental effects. Since both, projectiles and fragments traverse the same detectors, the detection efficiencies essentially cancel in the above expression. The main correction factor arises from the finite acceptance of the detector system for some of the fragments. For each fragment species, the yield distribution projected onto the spatial coordinate perpendicular to both, the beam axis and the axis of the field of the dipole magnet, was constructed. This distribution was fully accepted by the detector system for fragments with a magnetic rigidity near that of the beam. Fragments with N/Z ratios differing considerably from that of the projectile, however, gradually escaped from the detector acceptance. Fragment cross sections were determined only if more than one half of the yield distribution was covered and thus a safe extrapolation was ensured. If such a correction for incomplete acceptance was required, the systematic error of the correction factor was estimated and added to the statistical one.

III. EXPERIMENTAL RESULTS

Fragment production cross sections could be determined for $^{17-21}$O projectiles and carbon, nitrogen, and oxygen fragments which include both stable and neutron-rich isotopes. The results obtained for the carbon target are quoted in Table I.

It is known that the target dependence of fragmention cross sections can be factorized. The factorization can be illustrated on the basis of the present results. Fig. 2 compares fragment cross sections obtained from the carbon target with those from the lead target for the case of the ^{20}O beam. Except for the one- and two-neutron removal channnels, the ratios of the fragment cross sections range between values of 1.8 and 2.9 with a mean value of 2.1 ± 0.1. For the lead target, the few-neutron removal cross sections are influenced by the electromagnetic excitation process which has been discussed in detail previously [16].
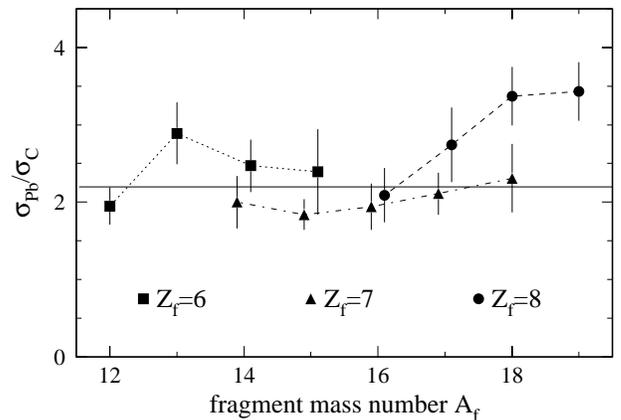

FIG. 2. Ratio of cross sections measured with a lead target to those measured with a carbon target yielding oxygen, nitrogen, and carbon fragments.

The ratio of 2.1 for the other isotopes is indicative of a more pheripheral nature of the nuclear fragmentation process. A scaling with the sum of projectile and target radii would yield a ratio of 1.7, a scaling with the target radius alone a ratio of 2.6. The latter value is the one used in EPAX.

For the stable beam ^{18}O, fragmentation cross sections have been measured at 1700 MeV/nucleon beam energy for beryllium and aluminum targets, see Ref. [17]. We include the experimental results for the beryllium target of Ref. [17] in Fig. 3 for comparison. The results of Ref. [17] agree with the present ones within maximum deviations of about 40 %. A certain trend towards larger cross sections for oxygen fragments and lower cross sections for carbon fragments observed in Ref. [17] with a beryllium target in comparison to the present results with a carbon target can be observed, while both measurements deliver almost identical cross sections for nitrogen fragments.

IV. MODEL CALCULATIONS

In the following, we compare the measured cross sections with those obtained from the empirical EPAX parameterization and with those obtained from abrasion-ablation models, see Fig. 3. First, we present a brief description of the physics underlying the various approaches.

EPAX parameterization. The EPAX parameterization follows similar earlier approaches by Rudstam or Silberberg, Tsao, and coworkers (see references in [2]). It assumes that for each fragment mass A_f the nuclear charges Z_f are distributed according to a skewed Gaussian curve around the central value; the location of the center and the width follow smooth analytical functions of A_f. The

TABLE I. Fragment production cross sections obtained from this experiment with the carbon target. Cross sections are quoted in millibarn.

Fragment / Beam	^{17}O (629 MeV/nucleon)	^{18}O (573 MeV/nucleon)	^{19}O (635 MeV/nucleon)	^{20}O (585 MeV/nucleon)	^{21}O (557 MeV/nucleon)
^{16}O	55.0 (6.6)	41.4 (3.0)	23.1 (2.5)	13.5 (2.2)	
^{17}O		53.5 (3.6)	17.2 (2.6)	17.2 (2.4)	
^{18}O			66.1 (5.5)	46.7 (4.9)	23.2 (13.2)
^{19}O				72.0 (7.4)	35.4 (7.0)
^{20}O					90.2 (13.8)
^{13}N	6.0 (2.0)	1.7 (0.4)			
^{14}N	25.6 (4.4)	18.7 (1.8)	10.4 (1.4)	5.4 (0.9)	
^{15}N	56.1 (9.4)	57.3 (3.9)	43.3 (3.7)	36.4 (2.9)	14.2 (3.1)
^{16}N	21.4 (3.8)	27.0 (3.7)	23.1 (2.3)	19.6 (2.0)	19.4 (3.6)
^{17}N		29.6 (2.2)	27.6 (3.3)	33.6 (2.9)	18.8 (3.3)
^{18}N			14.3 (2.3)	13.9 (2.2)	36.2 (8.5)
^{19}N				27.2 (3.1)	38.1 (13.1)
^{11}C	4.8 (2.0)				
^{12}C	32.1 (4.5)	17.4 (1.6)	14.0 (1.7)	8.8 (1.0)	
^{13}C	28.0 (4.4)	27.5 (2.2)	20.7 (2.1)	15.9 (1.6)	
^{14}C	7.2 (2.5)	20.3 (1.6)	20.4 (2.1)	17.4 (1.4)	
^{15}C			5.4 (0.8)	6.7 (1.0)	
^{16}C				5.9 (1.2)	

total yields at each mass A_f are assumed to decay exponentially with increasing mass difference from the projectile. Correction factors model the more narrow isotope distributions close to the projectile and the influence of the neutron-to-proton ratio of the projectile on the fragment distribution (the "memory effect"). EPAX has been shown to reproduce measured fragmentation cross sections from heavy-ions with masses above ^{40}Ar within a factor of about 2 [2]. For lighter projectiles, which are the subject of the present paper, the agreement with data can be expexted to deteriorate somewhat, since odd-even effects in the isotope distributions (which are not contained in the present EPAX version) can be shown to become increasingly important.

Abrasion-Ablation Models. Abrasion-ablation models describe fragmentation reactions as a two-stage process. In the abrasion stage of the reaction, the nucleons in the overlap region of two energetic heavy ions are scraped off (abraded) as the ions pass each other. In the subsequent ablation stage, the excited projectile and target fragments decay by statistical particle emission. One of the first models of this kind was developed by Bowman, Swiatecki and Tsang [3]. They used the geometrical overlap of two colliding spheres to determine the mass of the primary fragment and estimated its excitation energy as the difference in the surface energy of the abraded fragment and that of a sphere of equal volume. Although the model roughly described the overall characteristics of the data, it systematically placed the fragment mass distribution at larger values of the mass than those observed experimentally.

Later work used the Glauber approximation [19] to improve the description of primary fragment formation but concluded that the principal defect of the model was its low estimate of the primary excitation energy, which inhibited particle emission in the subsequent ablation stage [18].

More recently, two attempts have been made to improve the estimate of primary energy deposition by using a consistent independent-particle picture of the abrasion process [4,5]. The basic premises of these works are 1) that the collisions between projectile and target nucleons result in a primary fragment in which nucleons have been knocked out of some subset of the initially occupied independent-particle orbitals and 2) that the excitation energy of this configuration can be estimated as the energy of the corresponding particle-hole configuration of this primary fragment.

In Ref. [4], the geometrical formulation of the abrasion model, which distinguishes between a participant and two spectator zones [3], was combined with the independent-particle picture to predict the mass and nuclear-charge distribution [20], the excitation energy, and the angular momentum [21] of the spectators. An additional contribution to the excitation energy from interactions of the spectators with nucleons from the participant zone was deduced from experimental data [22]. The ablation stage was calculated within an evaporation model, where the emission of neutrons, protons and alpha particles is considered. Binding energies from the finite-range liquid drop model including microscopic corrections [23] are used in combination with level densities based on the
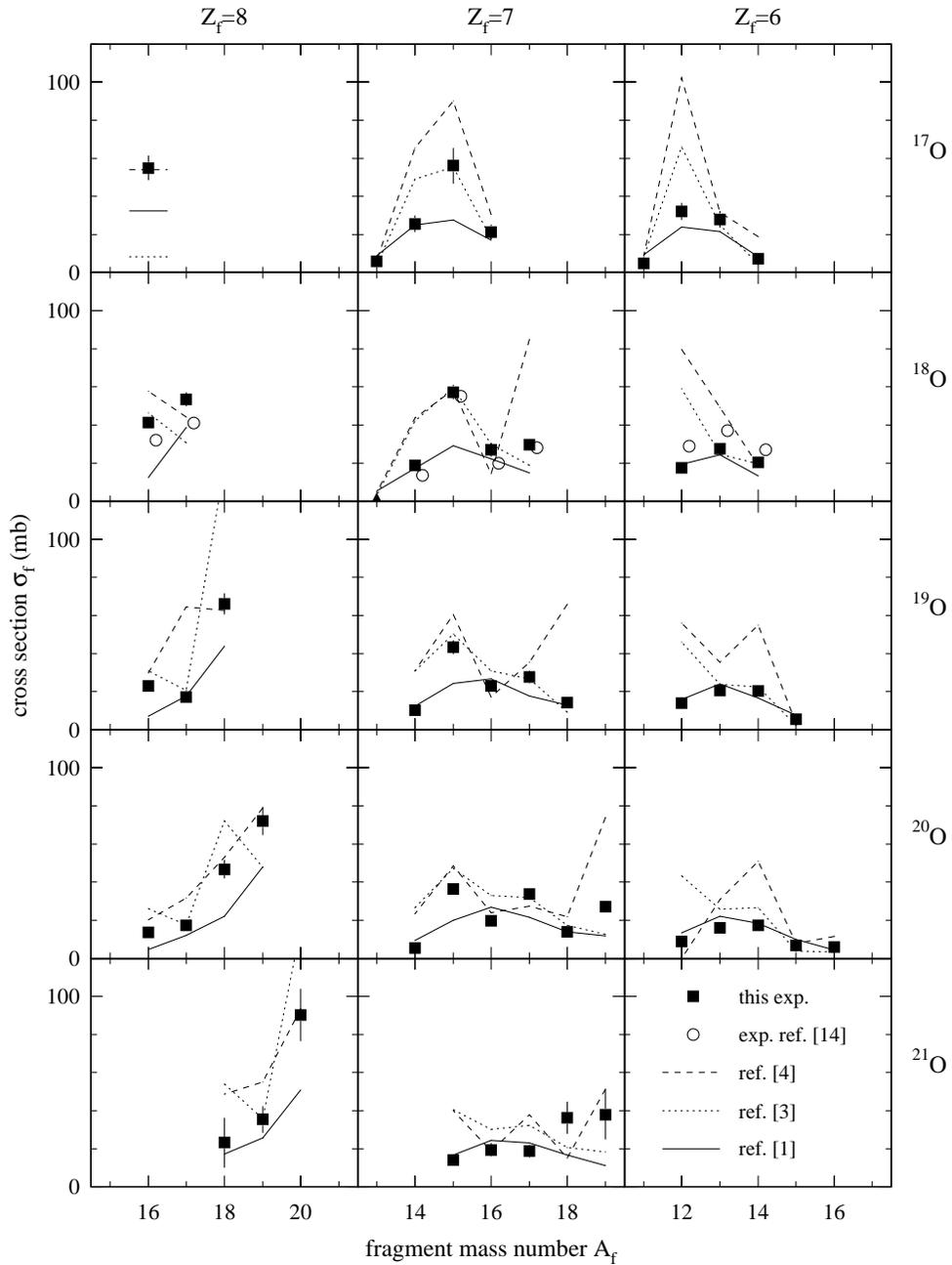
FIG. 3. Cross sections of projectile fragments with nuclear charges Z_f and masses A_f produced from $^{17-21}$O beams in a carbon target. In case of the ^{18}O beam, experimental results obtained in [17] for ^{18}O beams of 1700 MeV/nucleon on a Be target are included. The experimental cross sections (symbols) are compared to those calculated using various models: Two abrasion-ablasion models (dashed line from [5], dotted line from [4]). The solid line shows the results of the empirical EPAX parameterization [2].

5

Fermi-gas model with pairing correlations, shell effects, and collective contributions included [24–26].

The model of Ref. [5] attempts to provide a completely microscopic independent-particle model of the abrasion process. A survival probability is calculated for each single-particle orbital at each value of the impact parameter, as an overlap between the projectile orbital and its interaction with the target. These are combined to obtain the probability for the formation of a fragment in which a particular subset of the orbitals remains occupied. The excitation energy of the fragment is taken to be the particle-hole energy of the configuration relative to the ground state of the fragment. When the many combinations of orbitals that can lead to a fragment with the same mass number and charge are summed and then integrated over impact parameter, one obtains the differential cross section for the formation of that fragment as a function of the excitation energy. In the ablation stage of the model, it is assumed that the fragments decay by (multiple) statistical particle emission from an equilibrated primary fragment. Any pre-equilibrium effects that might be associated with the original particle-hole description are neglected. The ablation calculations are performed using the Weisskopf-Ewing evaporation formalism in which angular momentum conservation is neglected [27].

In the actual calculations using this model as presented below, harmonic oscillator wavefunctions with a characteristic energy of $\hbar\omega = 40/A^{1/3}$ MeV are used for the projectile states. The single-particle energy levels are obtained from a spherical Nilsson scheme with the same characteristic energy but including spin-orbit splitting and an $\vec{l} \cdot \vec{l}$ shift. The optical potential used to calculate the survival probabilities, is estimated within the impulse approximation. Differences between neutron and proton target densities are taken into account, although the same geometry is used for the two. The emission of gammas, neutrons, protons, and alpha particles is taken into account in the statistical decay of the ablation stage. The giant dipole resonance is assumed to dominate the γ emission. Cross sections for particle emission are obtained from global fits to reaction cross sections. The calculations use low-energy constant-temperature level densities matched to higher-energy Fermi-gas ones with level density parameters of $a \sim A/7$ MeV^{-1}, pairing shifts of $12/\sqrt{A}$ MeV, and experimental ground-state masses.

V. DISCUSSION

As can be seen from the full lines in Fig. 3, the EPAX parameterization seems to reproduce the general trend of the data rather well. While, as known, few-nucleon removal channels are less accurately predicted, the comparison for, e.g., carbon fragments is almost perfect. Though

the EPAX formula was obtained by adjusting to fragmentation data of stable beams only, the overall very good, almost quantitative description indicates that the parameterization of the "memory effect" is valid also for unstable projectiles as neutron-rich as ^{21}O ($A/Z = 2.625$). This confirms the previous observation by Sümmerer and Blank [2] that the fragment distributions for somewhat less neutron-rich secondary beams like ^{28}Mg ($A/Z = 2.333$) and ^{43}Ar ($A/Z = 2.389$) are well reproduced over more than one order of magnitude in cross section.

An obvious deficiency of the EPAX parameterization, however, is the fact that the odd-even effects, observed in our data particularly for the nitrogen fragments, cannot be reproduced. This is expected since the EPAX parameterization does not contain any physical description and no attempt has been made to parameterize the odd-even effects. The experimental data show that isotopes with even neutron numbers, especially ^{15}N with a closed N=8 shell, are more abundantly produced than their neighbors with odd neutron numbers. Likely, the large difference in neutron separation energy between unpaired and paired neutrons is responsible for the even-odd staggering in the production cross sections. This is illustrated by quoting the one-neutron separation energies of the ^{15,16,17,18}N isotopes which amount to 10.8, 2.5, 5.9, and 2.8 MeV, respectively. The unpaired neutron in ^{16}N or in ^{18}N is thus easily removed at the end of the evaporation chain, explaining their lower production cross sections in comparison to ^{15}N or ^{17}N, respectively.

Even-odd effects in the production cross sections are predicted by both formulations of the abrasion-ablation model as seen from Fig. 3. Apparently, both calculations, however, overestimate the effects. Nevertheless, the results, in general, agree with the experimental data within roughly a factor of two.

When comparing the general behavior of the data with the different model calcuations, all models reproduce the tendency of the measured cross sections as a function of neutron number of the reaction products reasonably well. In the range which is accessible to this experiment, systematic discrepancies between the empirical parametrization and the results of the abration-ablation models which are reported in Ref. [8] for heavier extremely neutron-rich fragmentation products are not observed.

VI. CONCLUSION

A systematic study of projectile fragmentation was performed for unstable, neutron-rich beams, here the oxygen isotopes up to ^{21}O. The experimental data could be reproduced by an empirical parameterization based on fragmentation data from stable nuclei. The trend towards more neutron-rich fragments with increasing neutron excess of the unstable beam seems to be well reproduced. Nuclear structure effects, however, seem to

influence the cross sections leading to odd-even effects which can qualitatively be accounted for in descriptions using abrasion-ablation models.

VII. ACKNOWLEDGEMENTS

[1] C.A. Bertulani, M.S. Hussein, G.Münzenberg, Physics of Radioactive Beams, Nova Science, New York (2001);

[2] K. Sümmerer *et al.*, Phys. Rev. **C42**, 2546 (1990); K. Sümmerer and B. Blank, Phys. Rev. **C61**, 034607 (2000).

[3] J.D. Bowman, W.J. Swiatecki and C.F. Tsang, LBL Report LBL-2908, 1973 (unpublished).

[4] J.J. Gaimard and K.-H. Schmidt, Nucl. Phys. **A531**, 709 (1991).

[5] B.V. Carlson, M.S. Hussein and R.C. Mastroleo, Phys. Rev. C **46**, R30 (1992); B.V. Carlson, Phys. Rev. **C51**, 252 (1995).

[6] Y. Yariv and Z. Fraenkel, Phys. Rev. **C24** , 488 (1981).

[7] A. Ozawa *et al.*, Nucl. Phys. **A673**, 411 (2001).

[8] J. Benlliure *et al.*, Nucl. Phys. **A660**, 87 (1999).

[9] M. de Jong *et al.*, Nucl. Phys. **A628**, 479 (1998).

[10] K. Sümmerer *et al.*, Phys. Rev. **C52**, 1106 (1995).

[11] Scientific Opportunities with an Advanced ISOL Facility, USA, Nov. 1997

[12] EURISOL, RTD project, EU contract number HPRI-1999-CT-50001 (1999).

[13] An International Accelerator Facility for Beams of Ions and Antiprotons, Conceptual Design Report, GSI, Darmstadt, Nov. 2001

[14] J. Benlliure *et al.*, GSI-preprint 2000-41 (2000).

[15] H. Geissel *et al.*, Nucl. Instr. and Meth. **B70**, 286 (1992).

[16] A. Leistenschneider *et al.*, Phys. Rev. Lett. **86** (2001) 5442.

[17] D.L. Olson *et al.*, Phys. Rev. **C24**, 1529 (1981); D.L. Olson *et al.*, Phys. Rev. **C28**, 1602 (1983).

[18] J. Hüfner, K. Schäfer and B. Schürmann, Phys. Rev. **C12**, 1888 (1975).

[19] R.J. Glauber, Lectures in theoretical physics, Vol. 1, Lectures delivered at the Summer Institute for Theoretical Physics, Univ. of Colorado, Boulder, 1958, ed. W.E. Brittin and L.G. Dunham, (Interscience Publishers, NY, 1959) pp. 315-414.

[20] T. Brohm, K.-H. Schmidt, Nucl. Phys. **A569** (1994) 821

[21] M. de Jong, A. V. Ignatyuk, K.-H. Schmidt, Nucl. Phys. **A613** (1997) 435

[22] K.-H. Schmidt *et al.* Phys. Lett. **B300** (1993) 313

[23] P. Møller, J.,R. Nix, W.D. Myers, W.J. Swiatecki, At. Data Nucl. Data Tables **59** (1995) 185

[24] A.V. Ignatyuk, G.N. Smirenkin, A.S. Tiskin, Yad. Fiz. **21** (1975) 485

[25] A.V. Ignatyuk, Yu.V. Sokolov, Sov. J. Nucl. Phys. **17** (1973) 376

[26] A.R. Junghans *et al.*, Nucl. Phys. **A629** (1998) 635

[27] V.F. Weisskopf and D.H. Ewing, Phys. Rev. **57**, 472, 935 (1940).